Dielectric, magnetic and electromagnetic shielding properties of Poly-(3,4ethylenedioxythiophene)-maghnite associated with different fillers with any non-canonical shape

Sidi Mohamed Benhamou[a,d,*], Antonio José Lozano-Guerrero[b], Yemouna Madaoui[c], Juan Monzó-Cabrera[b], Mohammed Hamouni[d], Alejandro Díaz-Morcillo[b], Smain Khaldi[d]

[a]Département du Second Cycle, Filière Electrotechnique, Ecole Supérieure en Sciences Appliquées de Tlemcen, BP 165 RP Bel Horizon, 13000 Tlemcen, Algérie.

[b]Departamento de Tecnologías de la Información y las Comunicaciones, Universidad Politécnica de Cartagena, Cartagena (Murcia), 30202 Spain.

[c]Laboratoire de Chimie des Polymères, Université d'Oran Es-Senia, Oran, Algérie

[d]Laboratoire de Recherche sur les Macromolécules, Bloc Laboratoires de Recherche, Faculté des Sciences, Pôle Rocade, Tlemcen, Algérie.

[*]Corresponding author: e-mail: sm.benhamou@essa-tlemcen.dz

Abstract: A new inverse measuring technique that corrects non-desired sample displacements and can handle any kind of sample shapes is presented. It is applied to the estimation of permittivity and permeability of Poly-(3,4ethylenedioxythiophene)-maghnite (PEDOT-Mag) associated with different additives such as iron, copper, and hydrogen. This electromagnetic characterization has been performed over the 9 to 11 GHz frequency range by comparing the simulated and measured scattering parameters of a partially filled WR-90 waveguide. Additionally, the reflection, absorption multiple reflection losses and the shielding effectiveness of these materials have been calculated. Results show higher values of dielectric constant and loss factor for PEDOT-Mag-copper, than those compounds associated with hydrogen or iron. As expected, the highest permeability values are achieved by PEDOT-Mag-iron. The composite PEDOT-Mag-copper exhibits higher attenuation constant, absorption loss, multiple reflection loss and shielding efficiency values than composites associated with iron or hydrogen. PEDOT-Mag-hydrogen, however, shows the highest reflection loss values.

Keywords: Inverse technique; electromagnetic shielding effectiveness; 3,4ethylenedioxythiophene-maghnite; electrically conductive additives.

1. Introduction

Dielectric permittivity and magnetic permeability properties of composites are of vital importance for several industrial applications and to infer their shielding capabilities. Consequently, determining the complex permittivity and permeability of materials is of great interest. There are many different measurement methods for different types of dielectric materials and different frequency bands, and all these methods have their own advantages and disadvantages [1]. These procedures can be divided into different classifications. For instance, resonant or non-resonant methods [2] can be distinguished attending to the use of a resonant electromagnetic (EM) structure or not. Also, these measurement techniques can be divided into transmission and/or reflection methods considering if they use for the EM properties determination the reflection coefficient and/or the transmission coefficient [3] in transmission lines such as waveguides or coaxial lines. Another classification can be made regarding the employed scenarios such as open or free space set-ups or closed configurations mainly in waveguide lines or cavities. Additionally, measurement approaches can be classified as destructive or non-destructive methods considering whether the sample needs a specific shape to be measured or it does not. The accuracy of each technique depends mainly on the frequency band, the material EM properties and the selected method [4]. Some of them provide more accurate results for low losses while other ones are better for high losses. When the material is solid, transmission or reflection methods employing waveguides or coaxial lines are usually applied for the measurement of the complex permittivity and permeability [5]. For liquid materials it may be more interesting the usage of open coaxial probes [6].

Practical advantages can be found when working with rectangular waveguide measurements to characterize electrically a material, for instance: the ease of sample manufacturing and employing relatively small samples when comparing to free space measurements where dimensions must be large enough to avoid corner effects. This is especially important when only small amounts of the material are available due to technical or economic reasons [7]. Transmission waveguide techniques involve estimating the permittivity and permeability of the samples from the measurement of the S parameters. In this case, the samples whose permittivity and permeability are to be measured, are introduced in a waveguide holder and two coaxial to rectangular waveguide transitions must be used. The rectangular waveguide must be excited in monomode conditions and the transitions and cables must be calibrated to eliminate their influence on the S parameters of the whole system [8]. Inverse techniques have become widespread in the determination of electromagnetic properties from scattering parameters, especially when the sample cannot be mechanized with canonical shapes. The retrieval of permeability and permittivity with inverse methods can be performed by using analytical expressions [9] or with numerical methods that closely model the EM structure [10]. The use of an optimization method is, however, always required for these techniques.

Owing to their dielectric and magnetic promising properties, the conductive polymer composites (CPCs) have become very interesting candidates as shielding materials. In some applications it is not only important to shield but also to avoid (or reduce) possible resonances from signals that can go inside the equipment (for instance, through vent holes or other slots in electronic equipment). In that situation a proper combination of external shielding and losses at the inner walls of the shield is very useful in order to damp possible resonances and CPCs can play an important role to achieve this. In some electronic systems, the material for electromagnetic interference (EMI) shielding purposes besides being effective, must be lightweight and flexible, especially in applications such as aero-space electronics, aircrafts and automobiles. When compared to metals, CPCs are competitive, specially, in EMI shielding applications for their good physical features such as the density and flexibility [11]. CPCs are produced by combining reinforcing charges with a polymer matrix. By means of this combination of charges, better characteristics are obtained than the ones shown by the original polymer and CPCs are increasingly being employed as a replacement of heavier metallic materials.

Previously, in [12] and [13] nanocomposites were formed adding conductive particles like aluminum and silver to clay and the electromagnetic shielding properties studied. In [14], [15] and [16] multiwall carbon nanotubes (MWCNT) were used as filler to increase the electrical conductivity. The clay is able to improve the thermal and sensory properties of polymer nanocomposites and the insertion of polymer monomer betwixt clay layers boosts the electrical conductivity of the clay-polymer nanocomposites [13]. Researchers have determined that the incorporation of metal fillers in the clay alters its electromagnetic properties. The intrinsic conductivity of the metal fillers, the clay dielectric constant and aspect ratio impacts greatly on the EM characteristics of metal–clay composite. The addition of metal/clay nanoparticles in polymers leads to composites that display excellent and auspicious magnetic, electrical, optical or mechanical properties [12]. The combination of a core and a shell using different dielectric/magnetic materials and forming microspheres or yolk-shell structures and paying attention to the air void to provide better absorbing/shielding properties in wider frequency ranges has gained attention recently [17], [18], [19], [20], [21]. In all these studies the permittivity and permeability of the samples is obtained using the Nicholson-Ross-Weir technique [3] applied to the scattering parameters. However, in this study, we provide a new measurement technique to obtain the permittivity and permeability from the measurement of scattering parameters of waveguides that contain samples with any kind of shape and minimizing the error that sample displacements can cause.

Currently, Poly-(3,4-ethylenedioxythiophene) (PEDOT) is one of these polymeric materials which plays a leadership role in antistatic, electric and electronic applications [22]. Previous results for this study were presented in [23], but only for a Sodium additive. A review of the benefits and shielding properties of conductive polymers are described in detail in [24], [25].

In this work, due to the small size of the samples and the working frequencies, a rectangular waveguide working in the TE_{10} monomode region is used. The reflection and transmission parameters have been employed to compute the relative permittivity and permeability of 3,4ethylenedioxythiophene non-canonical sheets associated with maghnite and three electrical charges: iron, copper and hydrogen in the 9–11 GHz frequency range. Since the shape of the samples could not fit the complete cross-section of the waveguide they had to be adapted to the inner section without completely filling it. That is the reason why we have selected an inverse technique which uses a numerical method that can deal with any particular sample shape. The optimization technique selected is Genetic Algorithms. It is a well-known technique that allows the reach of a global optimum avoiding secondary optimum values. However, it is time consuming and its use jointly with numerical methods is becoming possible during the last years due to the fast improvement in computation capabilities.

2. Materials and Methods

2.1. Synthesis of the composites

Composite materials have been manufactured using in situ oxidation chemical polymerization method. For the first material, ethylenedioxythiophene monomer is catalyzed by Maghnite-H^+ [26], while for the second, and third composites, the monomer is catalyzed, respectively, by Maghnite-Fe^{3+} and Maghnite-Cu^{2+}. Figure 1 shows a scheme of the synthesis process of PEDOT-Mag-(H^+, Fe^{3+}, Cu^{2+}). As shown in figure 1, the synthesis was carried out, reacting 0.5 g of 3,4 ethylenedioxythiophene (EDOT) liquid, plus 5% by weight of Maghnite (Mag); a type of Algerian clay [26] and hydrogen (H^+). After agitation for half hour, the liquid PEDOT seeps between filler-exchanged maghnite layers. According to the schematic image for Poly-(3,4ethylenedioxythiophene)-maghnite associated with different fillers illustrated in figure 2, the polymerisation processes are triggered by adding 0.1 mol of copper chloride (oxidizing agent). The mixture changes, over the course of 24 hours at room temperature, from colourless to green and finally to black. The other composites are produced by changing the conductive filler H^+ with, copper (Cu^{2+}) or iron Fe^{3+}. The use of the clay maghnite to improve the thermal properties of the polymer is subject of other works [26], [27]. In this paper, however, our interest is focused in its electromagnetic properties in X-Band.

The composites were subjected to filtration and washing with distilled water until a negative test to the silver nitrate (Ag NO3) was obtained. This process was repeated several times to remove all adhering substances. A powdered sample was obtained after 15 days of drying at 60°C. This sample was then introduced into a press pellet machine and then extracted in the form of a rounded tablet. The dimensions of the fabricated composites can be seen in Table 1.

Samples	Diameter *d* (mm)	Thickness *t* (mm)
PEDOT-Mag-H^+	13.25	1.19
PEDOT-Mag-Fe^{3+}	13.26	1.18
PEDOT-Mag-Cu^{2+}	13.25	1.26

Table 1. Diameter and thickness of the composites.

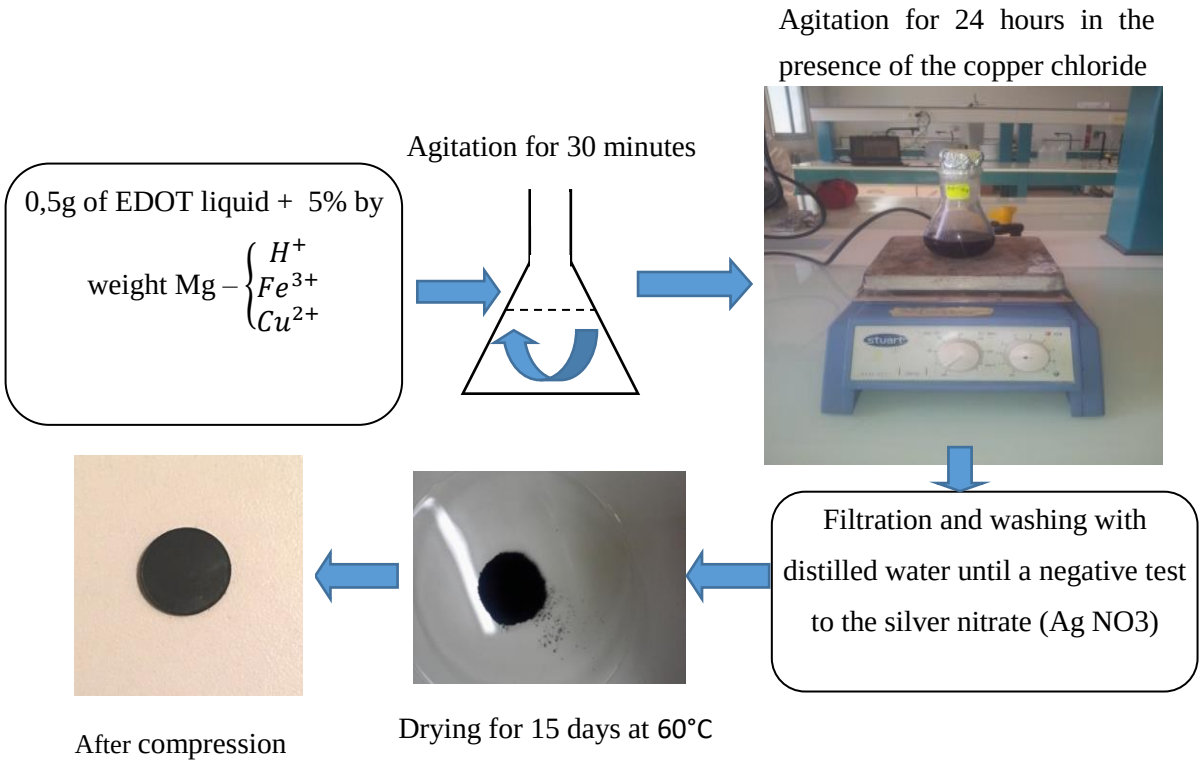

Fig. 1. Illustration of the synthesis process of PEDOT-Mag-(H^+, Fe^{3+}, Cu^{2+})

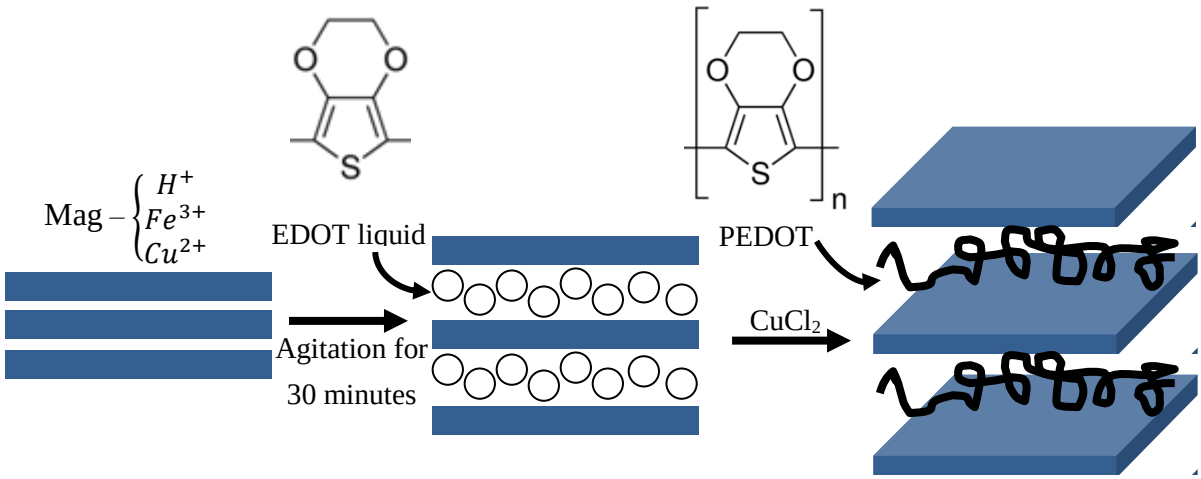

Fig. 2. Scheme of PEDOT-Mag-(H^+, Fe^{3+}, Cu^{2+}) elaboration

2.2. Measurement procedure of complex permittivity, complex permeability and shielding effectiveness

The electric permittivity (ε) is the physical property of a material that is associated with its energy storing capacity when a voltage difference is applied across it. This complex parameter is related to macroscopic properties like polarization or capacitance. Furthermore, the permittivity of a material directly connected to the speed at which an electrical signal can propagate through it [28].

The relative permittivity is a complex magnitude written as:

$$\varepsilon^* = \varepsilon' - j\varepsilon'' \tag{1}$$

where the real part of the relative permittivity, or dielectric constant, represents the mechanism of polarization and the possible storage of energy in the translational movement of the mobile charges that may exist and the imaginary part, ε'', also called loss factor, includes all the existing processes of energy loss [28].

Magnetic permeability is one of the magnetic characteristics which indicates how easily a magnetic material is magnetized [29]. The relative permeability, given by (2), represents the dynamic magnetic properties of magnetic materials:

$$\mu^* = \mu' - j\mu'' \tag{2}$$

The real part of relative permeability, μ', represents the capability of storage of the magnetic energy. The imaginary part μ'', or magnetic loss factor, takes into account the loss of magnetic energy [30].

To calculate the estimated permittivity and permeability of composite materials several techniques can be used: Nicholson-Ross-Weir, NIST iterative [3] or inverse techniques [10]. In this study, we obtained the results with an inverse technique by using the CST commercial software. CST commercial software was used in this process to simulate and evaluate each of the set ups jointly with the optimization technique of Genetic Algorithms. CST provided S_{ij} simulated complex scattering parameters, with i=1,2 and j=1,2, for several complex permittivity and permeability values of the material at the studied frequencies (9, 9.5, 10, 10.5 and 11 GHz) and these simulated results were compared to the measured ones in order to compute the fitness function in a similar way to that indicated in [31].

In figure 3 the flow diagram of the proposed inverse technique to measure the complex relative permittivity and permeability of materials is shown. Six unknowns are considered during the optimization procedure: complex permittivity and permeability of the sample, x (waveguide TE_{10} propagation direction) and z (waveguide transversal direction) displacement of the sample within the waveguide holder. The CST Microwave Studio inner built genetic algorithms procedure evaluates possible solutions or individuals using the fitness function (3). When the stop criterion for the fitness

function, in this case when all the generations have been computed during the GA, is accomplished then the optimization procedure stops and provides the best solution jointly with its fitness function value.

Since the samples where manually located within the waveguide holder and its position was measured with a digital vernier caliper some uncertainty was expected from this procedure. Therefore, the exact position of the samples was estimated by the GA in order to reduce the global uncertainty of the inverse measurement. This can be particularly important when frequency range for the measurements is high and can reduce the phase errors for S_{ij} when computing the evaluation function. We obtain effective values of the relative permittivity and permeability for homogeneous samples of Poly-(3,4ethylenedioxythiophene)-maghnite associated with several fillers through simulations and inverse optimization techniques.

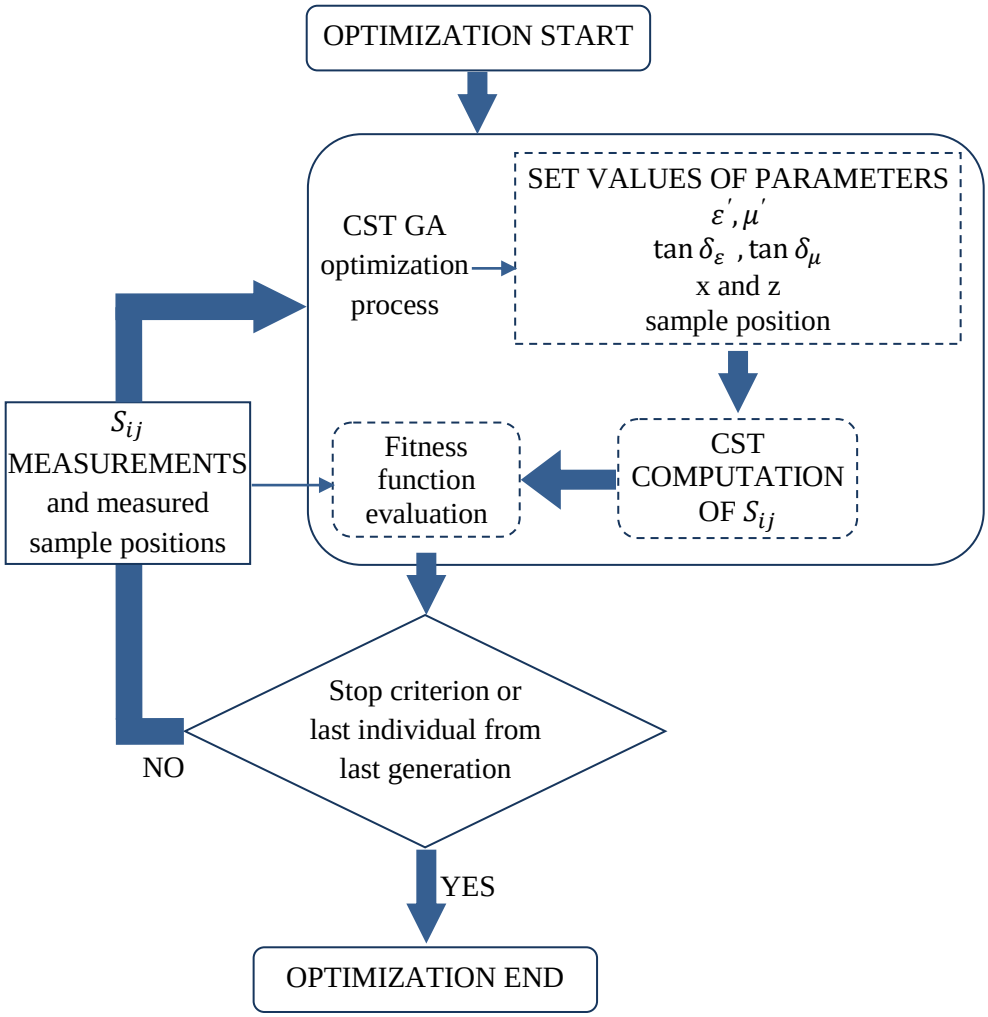

Fig.3. Flow diagram of the proposed technique to retrieve permittivity and permeability.

The fitness function used in this work is indicated in equation (3) and is similar to the ones in [10, 31]. It is computed only at five frequency points: 9, 9.5, 10, 10.5 and 11 GHz due to our computation capabilities.

$$fitness\ function = \sum_{i=1}^{2}\sum_{j=1}^{2}\left|\Re\left(S_{ij}^{meas}\right) - \Re\left(S_{ij}^{sim}\right)\right| + \left|\Im\left(S_{ij}^{meas}\right) - \Im\left(S_{ij}^{sim}\right)\right| \quad (3)$$

This fitness function evaluates the differences between the real and imaginary parts of the 4 scattering parameters. Genetic algorithms implemented inside CST Microwave studio have been used with a configuration of a 512 population and 16 generations. Mutation rate has been set to 60%. The limits for the searched parameters are: [1-10] for the real part of the permittivity or permeability and [0-0.3] for the magnetic or electric loss tangent). The limits for the samples movement where restricted to +/-1 mm from they initial measured position both for the *x* and *z* axis. Relationship between the dielectric and magnetic loss tangents, used in the optimization procedure, and the respective loss factors can be respectively obtained from equations (4) and (5):

$$\tan\delta_e = \frac{\varepsilon''}{\varepsilon'} \quad (4)$$

$$\tan\delta_m = \frac{\mu''}{\mu'} \quad (5)$$

After the retrieval of the permittivity and the permeability of the samples from the scattering parameters, the shielding effectiveness of a semi-infinite sheet of material with *t* thickness under a plane wave incidence was calculated.

According to [32] the shielding effectiveness of an infinite sample, as seen in figure 3, can be decomposed as

$$SE\ (dB) = A + R + B \quad (6)$$

where *A*(dB) is the absorption loss, *R*(dB) is the reflection loss and *B*(dB) the multiple reflection losses.

The scheme of the SE study can be observed in figure 4, where E_I is the incident field, E_R is the electric field due to the reflection and E_T the one due to the transmission through the shield.

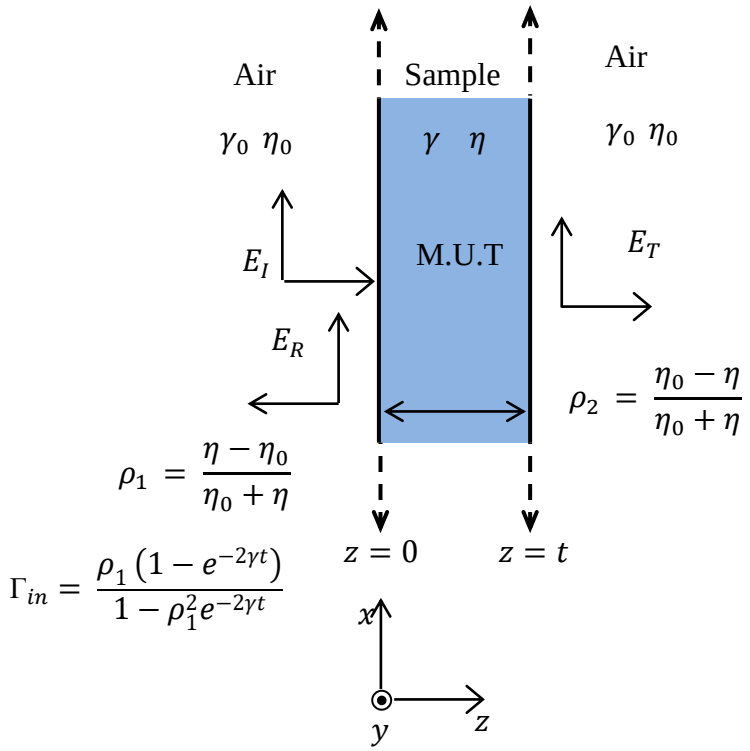

Fig.4. Set up of the shielding effectiveness study.

ρ_1 is the reflection coefficient of the wave travelling from the air to the material and ρ_2 from the material back to the air. The respective transmission factors can be obtained from:

$$T_1 = \frac{2\eta}{\eta+\eta_0} = 1 + \rho_1 \tag{7}$$

$$T_2 = \frac{2\eta_0}{\eta+\eta_0} = 1 + \rho_2 \tag{8}$$

The intrinsic impedance in the medium η can be obtained from [33] by using the permittivity and permeability values of the material

$$\eta = \eta_0\sqrt{\frac{\mu^*}{\varepsilon^*}} \tag{9}$$

where $\eta_0 = 120\pi\ \Omega$ is the vacuum intrinsic impedance.

As reported in [30] *SE*, *A*, *R* and *B* can be obtained as indicated in equations (10-13) using the Schelkunoff decomposition:

$$SE\ (dB) = -20\log_{10}\left|\frac{T_1T_2e^{-\gamma t}}{1-{\rho_1}^2e^{-2\gamma t}}\right| \tag{10}$$

$$A\ (dB) = -20\log_{10}|e^{-\gamma t}| \tag{11}$$

$$R\ (dB) = -20\log_{10}|T_1T_2| = -20\log_{10}|1-{\rho_1}^2| \tag{12}$$

$$B\ (dB) = -20\log_{10}|1-{\rho_1}^2e^{-2\gamma t}| \tag{13}$$

where t is the thickness of the sample and γ is the propagation constant in the sample can be obtained from [33]

$$\gamma = j\omega \frac{\sqrt{\mu^* \varepsilon^*}}{c_0} \tag{14}$$

where c_0 stands for the speed of light in vacuum. Thus, as seen from equations (10) and (14), the shielding effectiveness depends on the permittivity, permeability, frequency, and thickness of the sample. Since permittivity and permeability are intrinsic properties of the material the thickness of CPCs is usually the main design parameter for shielding purposes.

Additionally, the input impedance Z_{in} can also be obtained from the input reflection coefficient Γ_{in} in figure 3 from

$$Z_{in} = \eta_0 \frac{1+\Gamma_{in}}{1-\Gamma_{in}} \tag{15}$$

Reflection loss *R,* is usually referred as the primary shielding mechanism for metallic materials and provides an insight of how the EM shielding is obtained in the sample under test. The impedance difference between the free space and the material under study is the cause of the reflection loss and it is attributed to the existing mobile charge carriers and electric dipoles, which interact with the impinging electromagnetic fields. High value of the dielectric constant materials, shield mainly through the reflection mechanism. The absorption depends on several parameters such as the permittivity, the permeability, the sample thickness and the frequency of the electromagnetic wave [20]. The absorption loss, $A(dB)$, expressed in (16) can be derived from (11) to relate it to the attenuation constant and thickness of the material.

$$A(dB) = \alpha \cdot 8.68 \cdot t \tag{16}$$

where the attenuation constant α (Np/m) is the real part of γ and can be derived from equation [25]

$$\alpha = \frac{\sqrt{2}\pi f}{c_0} \cdot \sqrt{(\mu''\varepsilon'' - \mu'\varepsilon') + \sqrt{(\mu''\varepsilon'' - \mu'\varepsilon')^2 + (\varepsilon'\mu'' + \varepsilon''\mu')^2}} \tag{17}$$

where *f* is the frequency expressed in Hz.

To compute the conductivity of the CPC, the following expression has been used in this work.

$$\sigma = 2\pi f_0 \varepsilon_0 \varepsilon'' \tag{18}$$

2.3. Measurement set up

Scattering parameters (S-parameters) can be obtained using a VNA. Open field setups, anechoic or reverberant chambers are possible choices to measure the SE of a sample [34].The inverse measurement procedure involves comparing the transmitted and reflected signal in the presence of the composite for both the measured and simulated setups. The measurement process is carried out in [10] by injecting a signal of the appropriate frequency into a waveguide and there by measuring the S

parameters. In this work, however, we propose the use of a transmission/reflection waveguide setup for the measurement of the scattering parameters and the extraction of the EM properties. A WR-90 Agilent waveguide kit was used in the frequency range 9 to 11 GHz fed by a VNA Rohde & Schwarz ZVA67 to measure the reflection and transmission parameters. Selected frequencies allow to work in the monomode range of the waveguide kit. For the inverse measurements of magnetic and dielectric properties waveguide losses have been assumed negligible.

In figures 5a) and b), the experimental setup for measuring the permeability and permittivity of the studied materials can be observed. CPC samples are introduced in a 10 mm WR-90 waveguide holder between two coaxial to waveguide adapters. Those adapters are connected to the VNA ports. To remove the influence of the coaxial to waveguide transitions a de-embedding procedure using waveguide lines and shorts has been carried out as indicated in [33] to consider, uniquely, the scattering parameters of the holder with the sample. In figure 5c) it can be seen the CST Microwave Studio simulation set up scheme used in order to apply the inverse measurement procedure. As it can be observed, no WR-90 transitions were simulated since their effect was eliminated from the measurements during the de-embedding procedure.

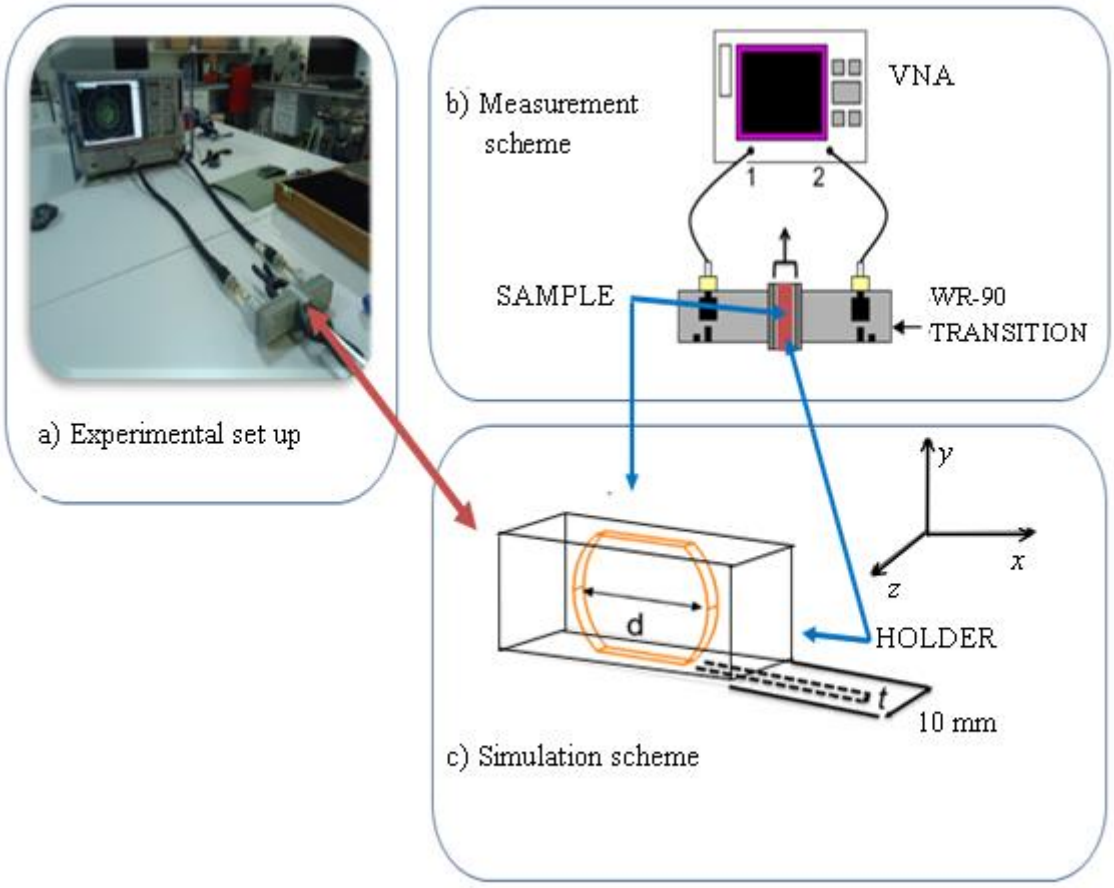

Fig.5. a) Experimental set up for the waveguide permittivity and permeability measurements, b) measurement scheme, and c) CST simulation scheme.

3. Results and Discussion

3.1. Dielectric and magnetic properties

In figure 6 we can observe the real and imaginary parts of electrical permittivity for the three different polymers studied in this work from 9 to 11 GHz at 5 discrete frequency points. The value for the air has also been obtained for sake of verification by using an empty holder, with no sample inside. From obtained results one can conclude that the value of ε' and ε'' is directly linked to the nature of the additive charges sincethe conductive charge added into a polymer composite enhances the values of the complex permittivity. It can be perceived that compared to the other composites, the PEDOT-Mag-Cu^{2+} composite shows higher real and imaginary permittivity average values ($\varepsilon' = 4.97$, $\varepsilon'' = 0.9$). Therefore, the PEDOT-Mag-Cu^{2+} exhibits a better ability to store the electric field energy and a higher capability for electric field absorption and attenuation of electromagnetic waves. The dielectric constants of the other two composites, PEDOT-Mag-H^{+} and PEDOT-Mag-Fe^{3+}, show a similar behavior with slightly lower mean values. The imaginary part stays stable within the whole frequency range although PEDOT-Mag-Cu^{2+} composite can dissipate more microwave energy in this frequency band.

Mean values of real and imaginary parts of the dielectric relative permittivity in the frequency band 9-11 GHz are listed in Table 2. Using equation (18) the mean values of the electrical conductivity for each composite are included, also, in Table 2. The obtained results indicate that better electrical conductivity values are obtained when the copper is used as filler. The second-best filler in terms of electrical conductivity is hydrogen and, lastly, iron. Compared to the other composites, PEDOT-Mag-Cu^{2+} exhibits a higher dielectric loss which obviously can be associated to a higher effect of electric conduction.

Sample	$\boldsymbol{\varepsilon'}$	$\boldsymbol{\varepsilon''}$	$\boldsymbol{\sigma}$ $(\boldsymbol{S/m})$
PEDOT-Mag-H^{+}	4.76	0.75	0.41
PEDOT-Mag-Fe^{3+}	4.34	0.58	0.32
PEDOT-Mag-Cu^{2+}	4.97	0.9	0.5

Table 2. Mean values of the relative complex permittivity and conductivities of composites within the 9-11 GHz frequency band.

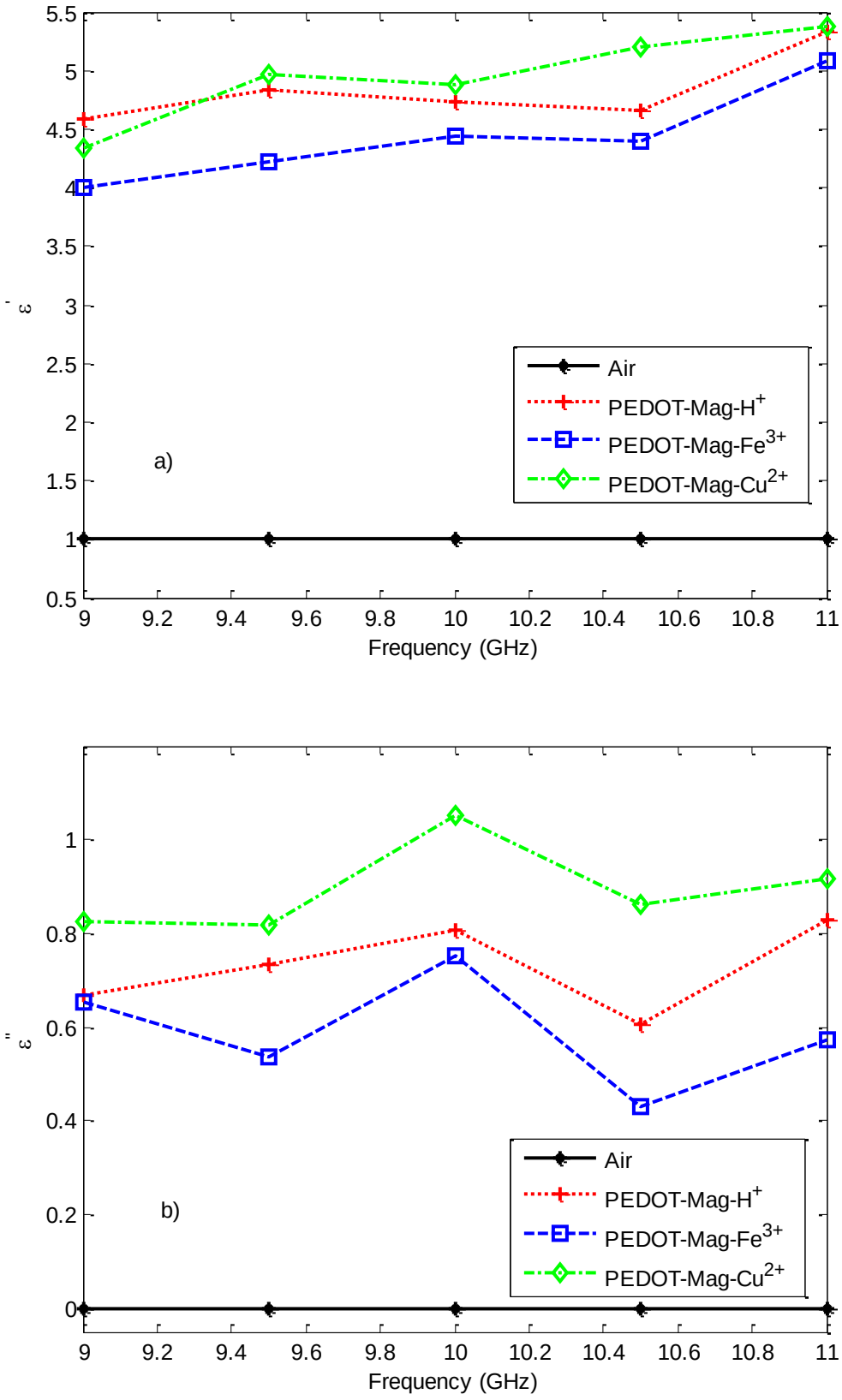

Fig.6. Real (a) and imaginary (b) parts of relative electrical permittivity of different samples.

The real and imaginary parts of the calculated relative permeability with the proposed inverse technique for the PEDOT polymers can be seen in figure 7. It can be observed that μ' and μ'' values exhibit important variations between 9 and 11 GHz and a strong dependence on the added charges. Values of μ' are in between 1 and 2.3 being the PEDOT-Mag-Fe^{3+} sample the one that exhibits higher values. Regarding magnetic losses, PEDOT-Mag-Cu^{2+} shows the highest values around 9 GHz, higher than 0.3, whereas PEDOT-Mag-Fe^{3+} shows the highest losses at 11 GHz. As expected, PEDOT-Mag-H^{+} shows the weakest magnetic behavior both for μ' and μ'' values. It should be noted that both μ' and μ'' values may be over estimated in the frequency range 9-9.5 GHz for all the PEDOT formulations since the air values are slightly higher than the real ones. This could be due to the calibration of the coaxial to waveguide transitions.

In figure 8a the values for the attenuation constant are represented following the formulation in equation (17). PEDOT-Mg-Cu^{2+} and PEDOT-Mag-Fe^{3+} are the samples with a higher attenuation constant. This is due to its association with the magnetic and dielectric loss factors, which are higher for those polymers. From figure 8b, which shows the input impedance plotted by using equation (15), we note that, the magnitude of the input impedance of PEDOT-Mag-H^{+} and PEDOT-Mg- Cu^{2+} is lower than PEDOT-Mag-Fe^{3+}.

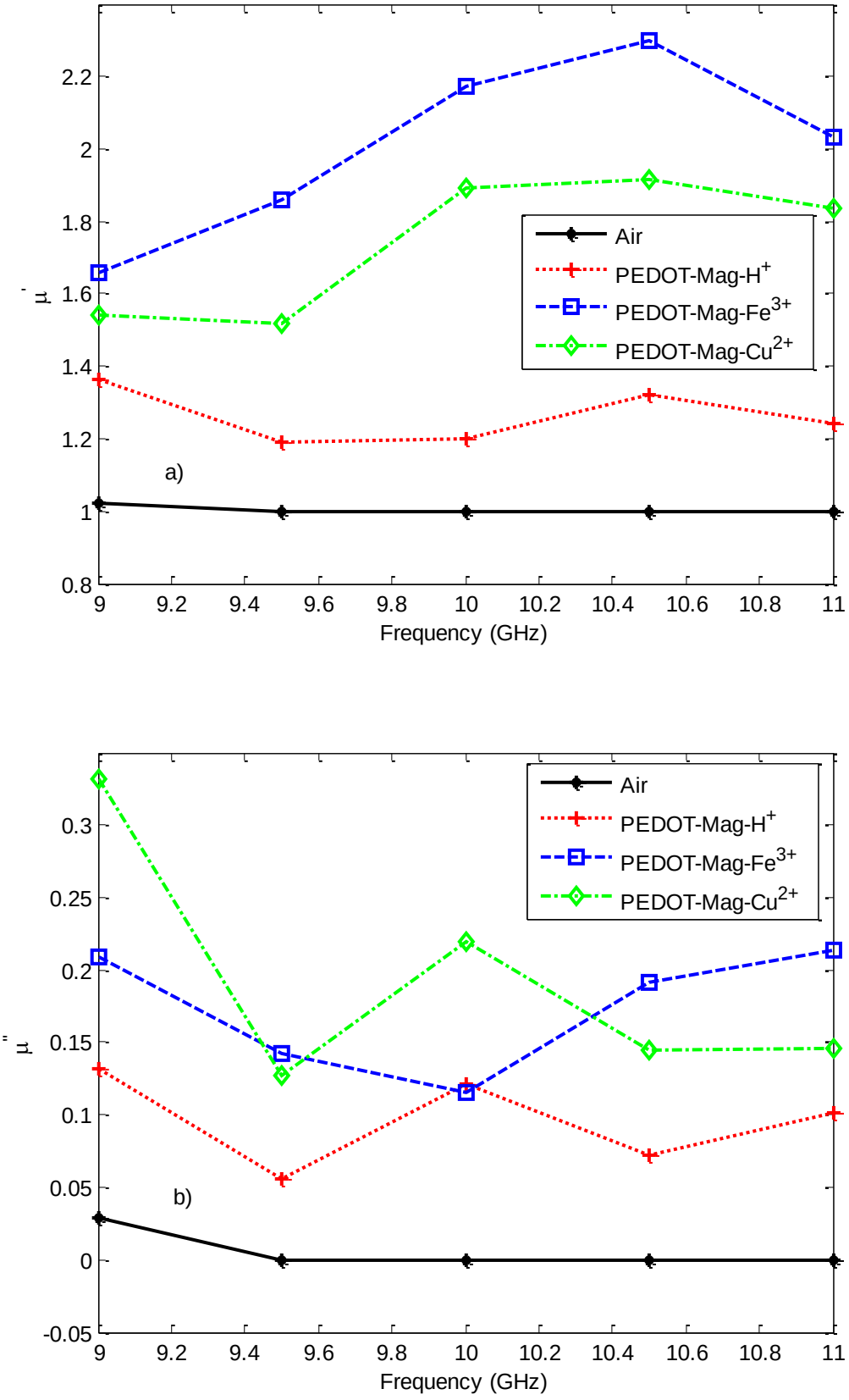

Fig.7. Real (a) and imaginary (b) parts of magnetic permeability of different samples.

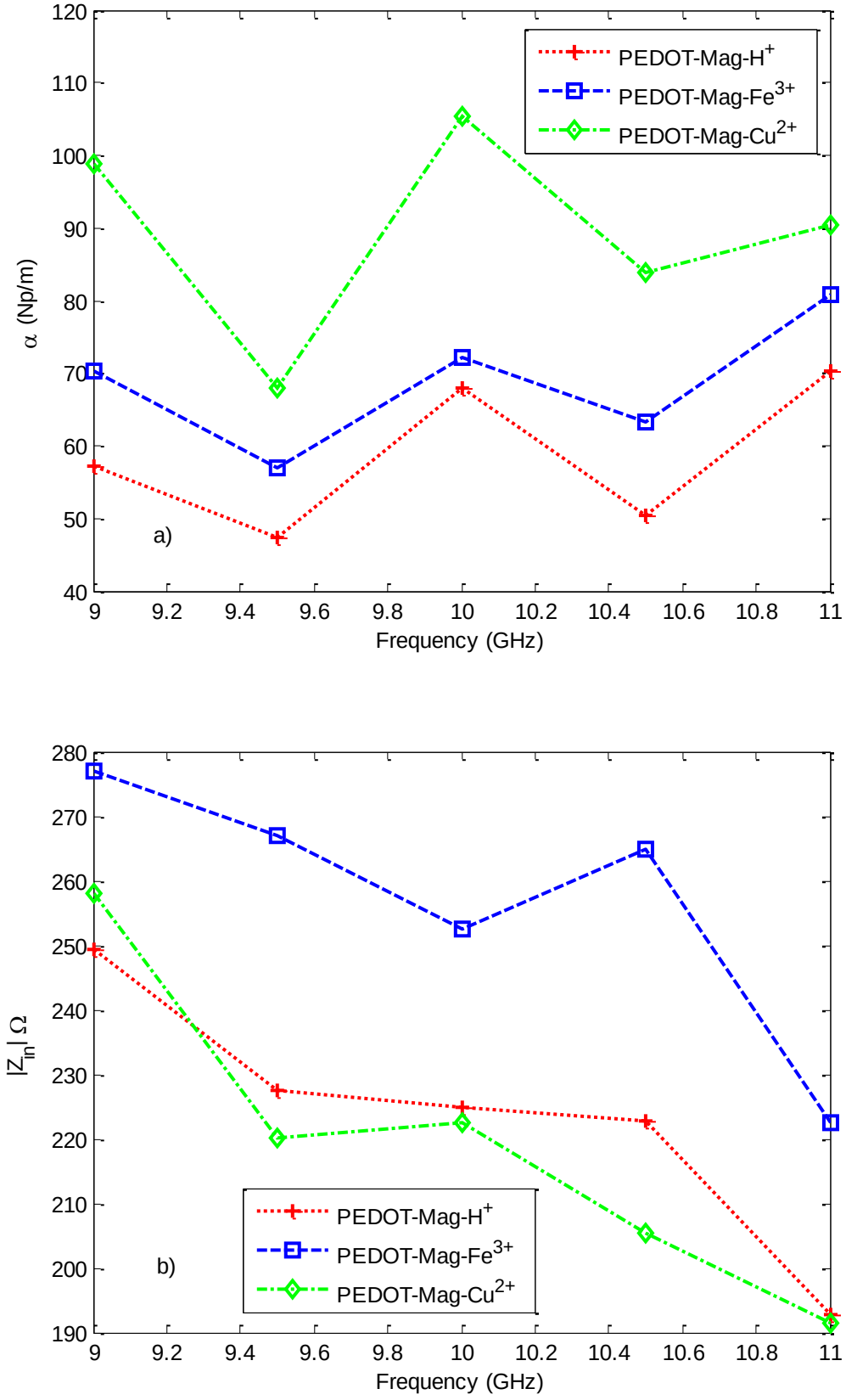

Fig. 8. (a) The attenuation constant and (b) the free space input impedance magnitude of the samples.

3.2. Electromagnetic shielding properties of manufactured materials

The reflection loss in free space, estimated by using the EM properties obtained with the inverse waveguide method, is shown in figure 9 for the frequency range of 9–11 GHz. Although PEDOT-Mag-H^+ has a better reflection loss compared to other composites, it can be perceived that the reflection loss of all the polymers is low. The reflection loss value of PEDOT-Mag-H^+ is around 1 dB while those of PEDOT-Mag-Fe^{3+} and PEDOT-Mag-H^+ composites are around 0.5 dB.

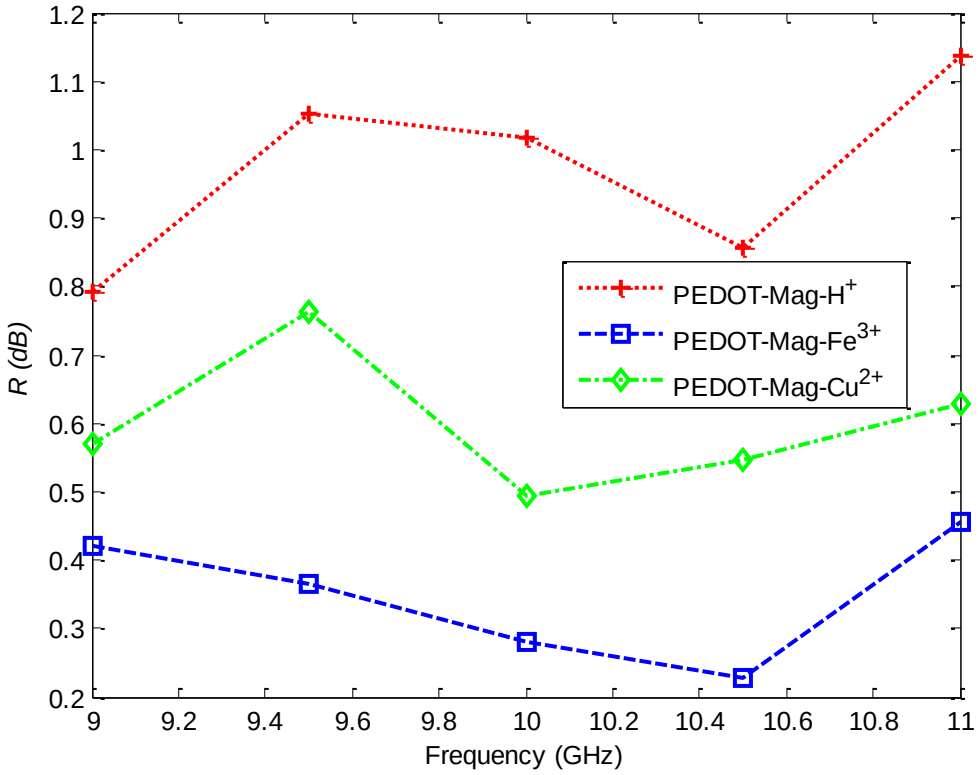

Fig. 9. Reflection loss of the studied polymer composites.

The absorption loss is also an important mechanism to provide an accurate shielding level and it is proportional to the thickness of the shield as shown in (16). Absorption is significant in the materials with high value of the dielectric constant and magnetic permeability. As all composites manufactured in this work show low magnetic properties, the absorption loss will depend mainly on the dielectric properties of the samples. Obtained results of the absorption loss according to (11) are shown in figure 10 the frequency range of 9–11 GHz. According to the electrical conductivity of materials, we have obtained a reasonable ranking of the absorption loss curves of different composites. The sample with the better electrical conductivity, namely PEDOT-Mag-Cu^{2+}, exhibits a better absorption loss while the PEDOT-Mag-Fe^{3+} and PEDOT-Mag-H^+ show lower values.

In figure11 the multiple reflection losses are represented. At some frequency, the internal reflection loss has a negative value thereby reducing the shielding effectiveness.

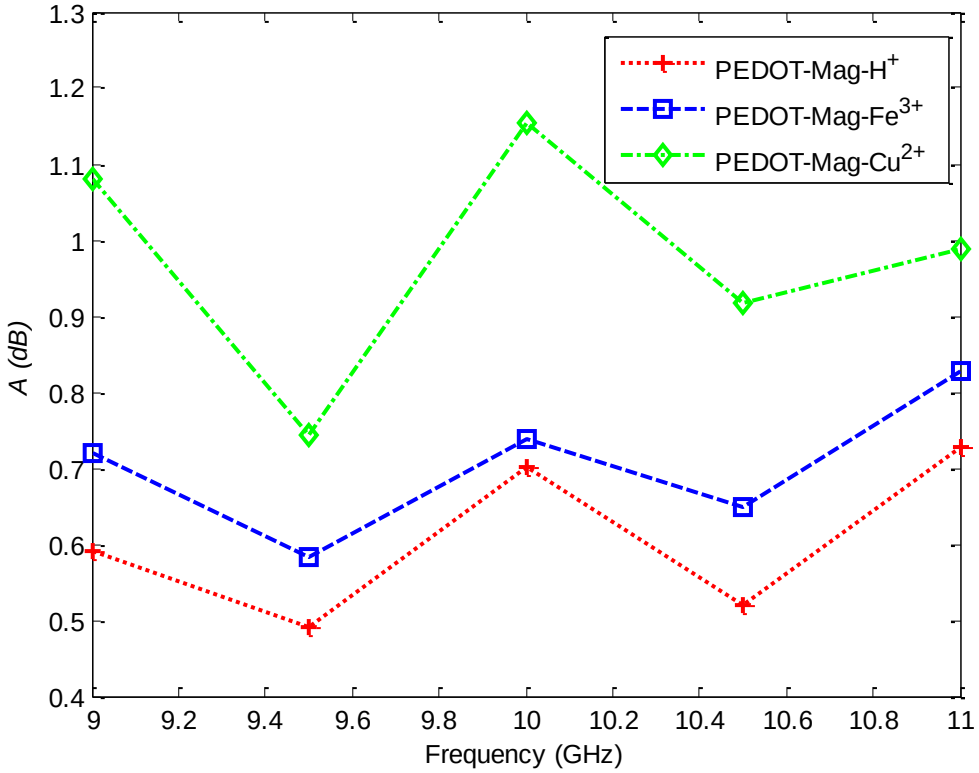

Fig. 10. Absorption loss of the studied polymer composites.

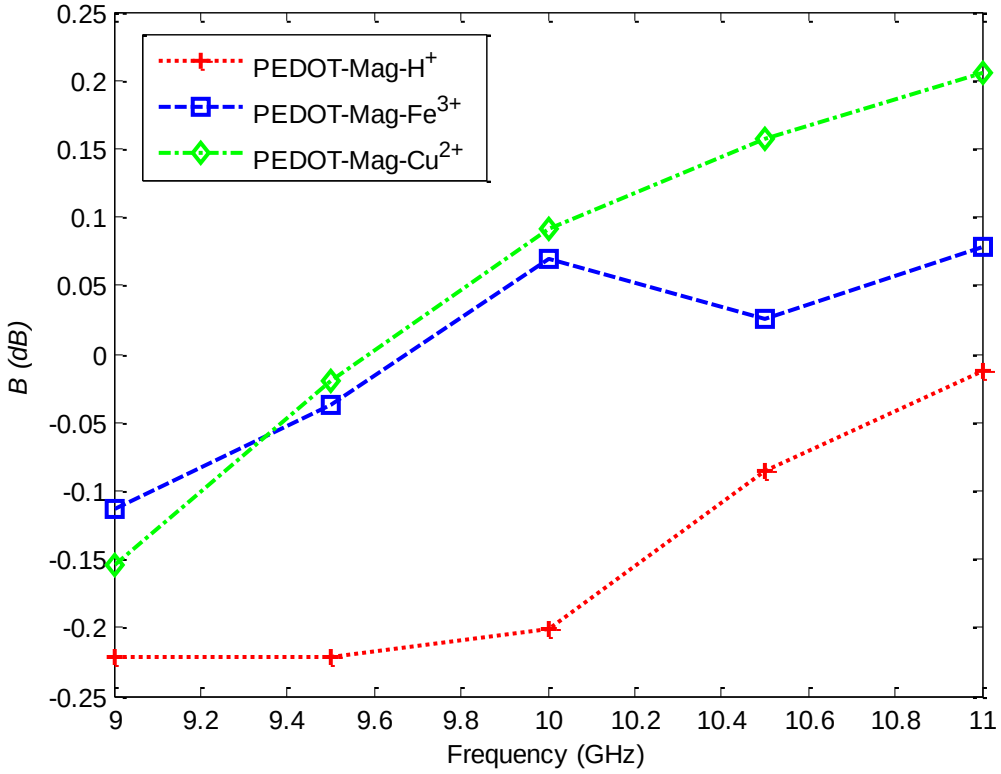

Fig. 11. Multiple reflection loss of the studied polymer composites.

In this work SE is defined as the sum of the reflection, absorption and multiple reflection losses as shown in equation (6). Figure12 illustrates the shielding effectiveness values of the polymers obtained in the frequency range of 9–11 GHz. Like the reflection and absorption losses, the shielding behavior of all the composites is highly influenced by the permittivity of the different samples. The SE of PEDOT-Mag-Cu^{2+} is the highest of the three studied polymers followed by the PEDOT-Mag-H^{+} and finally PEDOT-Mag-Fe^{3+}.

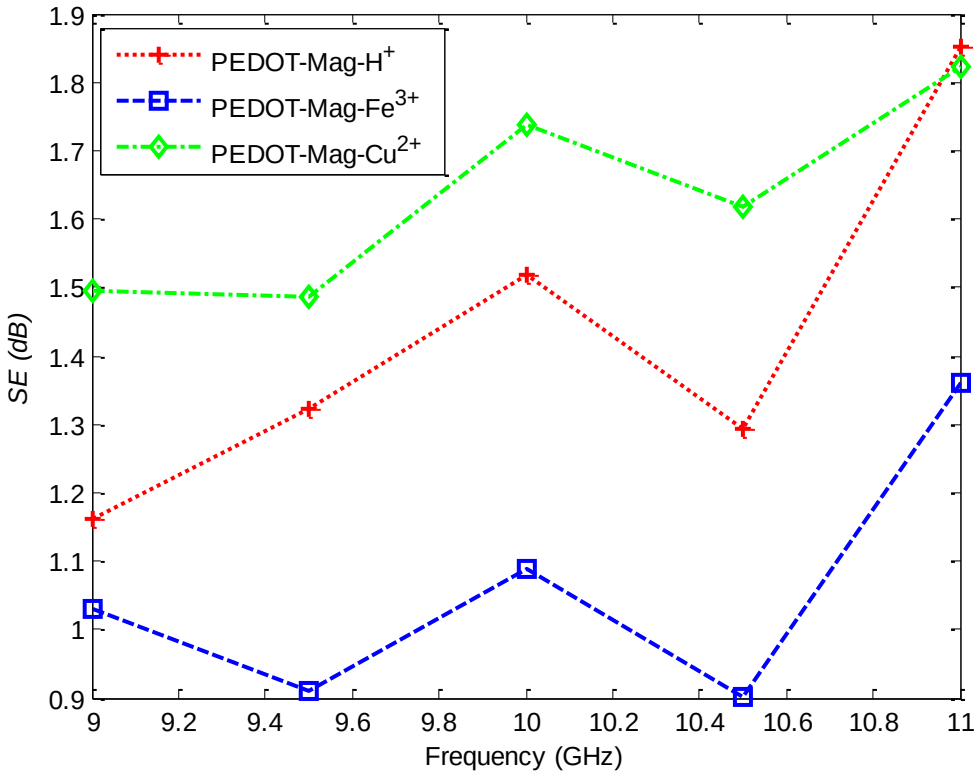

Fig. 12. Shielding effectiveness of the studied polymer composites.

In figure 13 the fitness function for the optimization process is provided for all the measured materials, also including the air. It can be perceived that all the fitness function values are at the same order of magnitude being the PEDOT-Mag-Cu^{2+} polymer the one with the best fitness behavior. Error incrementing the fitness function at each frequency has several sources such as: sample position (*x* and *z* variables), errors in the sample modelling: sample dimensions and shape, uncertainties during the coaxial-waveguide transition calibration, and uncertainties associated to the VNA measurement procedure.

To show the error in sample positioning, the optimized results for the sample displacement variable at the *x* and *z* axes, are represented in figures 14a) and fig. 14b), respectively. It can be observed that the results are more unstable for the *x* axis than for the *z* axis. However, one can conclude from results that the optimized movements from the initial sample positioning are always lower than 1 mm, which seems reasonable due to the manual positioning of the samples within the waveguide.

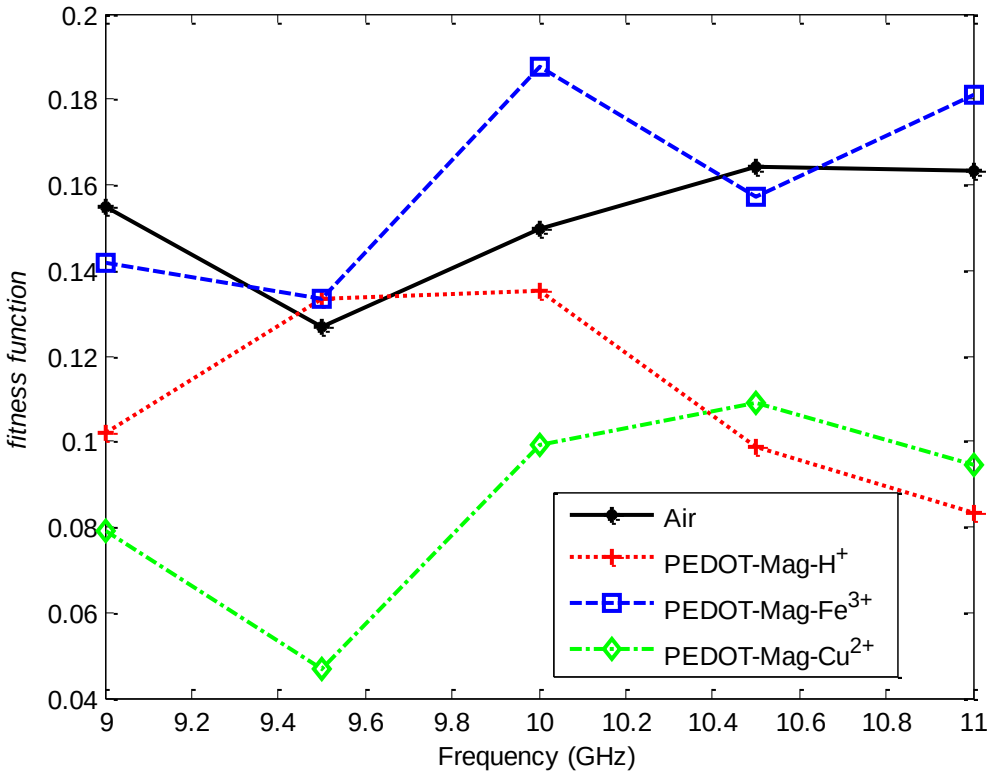

Fig. 13. Fitness function for the optimization process

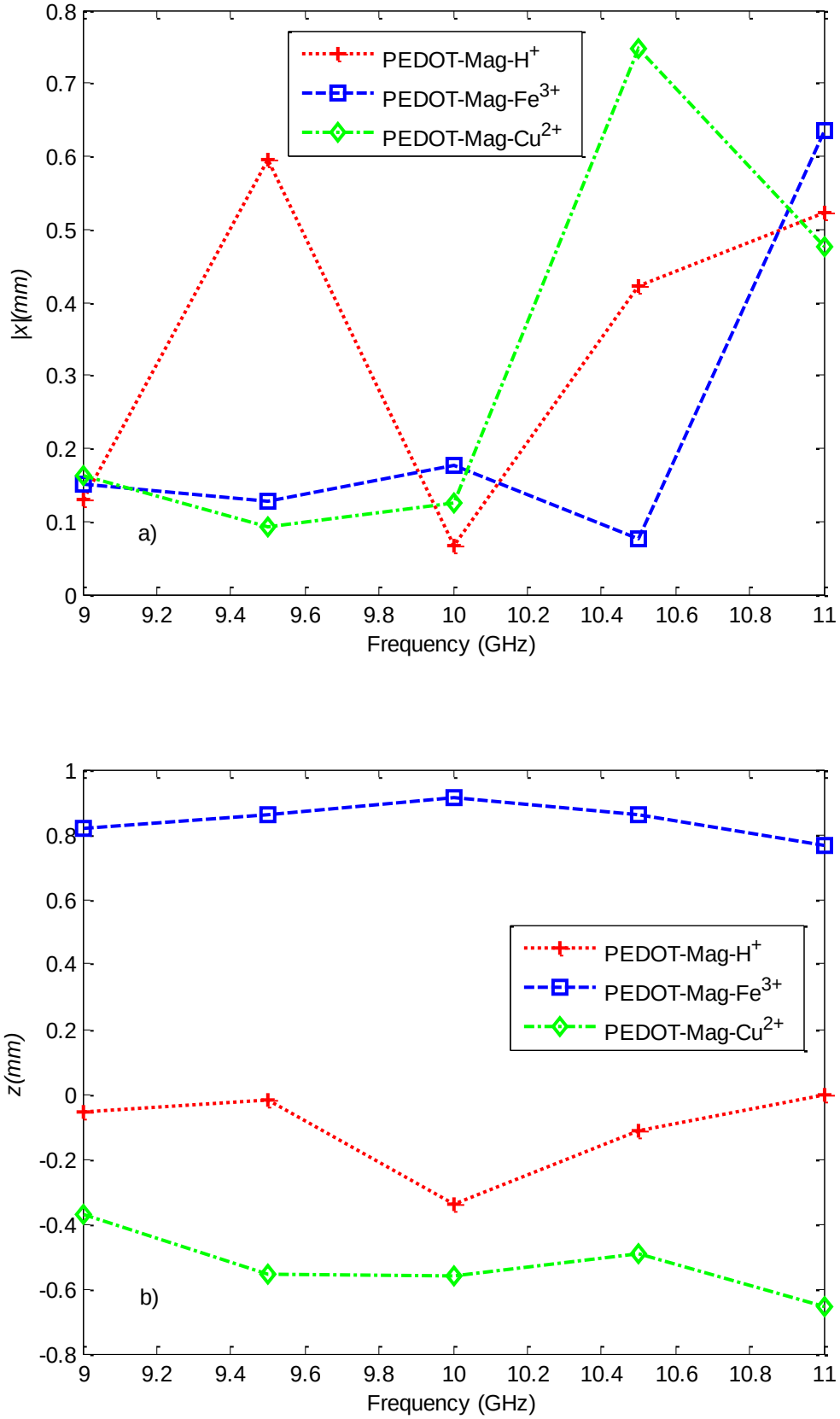

Fig. 14. a) *x* sample displacement from initial position b) *z* sample displacement from initial position after the optimization process

4. Conclusion

In this work an inverse technique to provide the permittivity, permeability and the sample position variation within a waveguide has been developed and employed to characterize the EM and shielding properties of PEDOTs with maghnite and three different additives. The proposed methodology is able to handle any kind of shape and sample positioning error and it can be applied to a high number of cases where analytical solutions cannot deal with the required set-ups.

Results are very stable for the permittivity while for the permeability, and especially for the imaginary part, show a higher variation and a lower accuracy. Concerning the sample positioning optimization, in this case, results show bigger variations in the TE_{10} propagation direction, *x* axis, than in the transversal position, *z* axis, being errors lower than 1 mm in all cases.

Regarding the behavior of the relative dielectric permittivity of the different compounds, it can be observed in figure 6 that the compound PEDOT-Mag-Cu^{2+} shows higher values of dielectric constant and loss factor than those compounds associated with hydrogen and iron within the measuring bandwidth.

In fact, the mean value of the dielectric constant for the PEDOT-Mag-Cu^{2+} sample is 14.5% higher than PEDOT-Mag-Fe^{3+} and 4.4% higher than PEDOT-Mag-H^{+}. The average loss factor of PEDOT-Mag-Cu^{2+} is 22% higher than the average value of PEDOT-Mag-H^{+} and 56% higher than PEDOT-Mag-Cu^{2+}.

A similar trend is perceived for shielding effectiveness in figure 12. Again, PEDOT-Mag-Cu^{2+} shows higher shielding effectiveness values than PEDOT-Mag-H^{+} and PEDOT-Mag-Fe^{3+}, mainly for frequencies below 10.5 GHz. The average SE for PEDOT-Mag-Cu^{2+} is around 15% and 56% higher than the average values of PEDOT-Mag-H^{+} and PEDOT-Mag-Fe^{3+}, respectively.

References

[1] R. N. Clarke, A. P. Gregory, D. Cannell, M. Patrick, S. Wylie, I. Youngs, G. Hill, A guide to the characterisation of dielectric materials at RF and microwave frequencies. Technical report published by institute of measurement and control (UK) / national physical laboratory, Characterization of Dielectric Materials atWR-15 band (50-75 GHz) using VNA-based Technique. 2003.

[2] J. Krupka, Frequency domain complex permittivity measurements at microwave frequencies, Meas. Sci. Technol. 17 (2006) 55-70.https://doi:10.1088/0957-0233/17/6/R01.

[3] J. Baker-Jarvis, M. Janezic, B. Riddle, R. Johnk, C. Holloway, R. Geyer, C. Grosvenor, Measuring the permittivity and permeability of lossy materials: solids, liquids, metals, and negative-index materials, Technical Note (NIST TN), National Institute of Standards and Technology, Gaithersburg, MD. 2005.

[4] J. Krupka, Measurements of the complex permittivity of low loss polymers at frequency range from 5 GHz to 50 GHz, IEEE Microw. Wirel. Compon. Lett., 26 (2016) 464-466. https://10.1109/LMWC.2016.2562640.

[5] E. Hidetoshi, I. Takao H. Osamu, Measurement method of complex permittivity and permeability for a powdered material using a waveguide in microwave band, Sci. Technol. Adv. Mater. 7 (2006) 77-83. https://doi.org/10.1016/j.stam.2005.11.019.

[6] A. Boughriet , Z. Wu , H. Mccann, L. E. Davis, The Measurement of dielectric properties of liquids at microwave frequencies using open-ended coaxial probes, in: 1 st World Congress on Industrial Process Tomography, 1999, pp. 318-322..

[7] L. Christer, D. Sjoberg, L. Elmkvist, Waveguide measurements of the permittivity and permeability at temperatures of up to 1000°C, IEEE Trans. Instrum. Meas. 60 (2011) 2872 – 2880. https://10.1109/TIM.2011.2122150.

[8] J. Vimal Vas, M. Joy Thomas, Electromagnetic shielding effectiveness of layered polymer nanocomposites, IEEE Trans. Electromagn. Compat. 60 (2018)376–384. https://10.1109/TEMC.2017.2719764.

[9] L. Ait Benali, A. Tribak, J. Terhzaz, A. Mediavilla Sánchez, An accurate method to estimate complex permittivity of dielectric materials at X-band frequencies, Int. J. Microw. Opt. Technol.15 (2020) 10-16. http://hdl.handle.net/10902/18653.

[10] M. E. Requena-Perez, A. Albero-Ortiz, J. Monzo-Cabrera, A. Diaz-Morcillo, Combined use of genetic algorithms and gradient descent optimization methods for accurate inverse permittivity measurement, IEEE Trans. Microw. Theory Tech. 54 (2006) 615-624. https://10.1109/TMTT.2005.862671.

[11] L. Zhang, N.T. Alvarez, M. Zhang, M. Haase, R. Malik, D. Mast, V. Shanov, Preparation and characterization of graphene paper for electromagnetic interference shielding, Carbon. 82 (2015)353–359.https://doi.org/10.1016/j.carbon.2014.10.080.

[12] M. P. Gashti, S. Eslami, Structural, optical and electromagnetic properties of aluminum–clay nanocomposites, Superlattices Microstruct. 51 (2012) 135-148. https://doi.org/10.1016/j.spmi.2011.11.008

[13] I. Ebrahimi, M. P.Gashti, Chemically reduced versus photo-reduced clay-Ag-polypyrrole ternary nanocomposites: Comparing thermal, optical, electrical and electromagnetic shielding properties, Mater. Res. Bull. 83 (2016) 96-107. https://doi.org/10.1016/j.materresbull.2016.05.024.

[14] R. Che, L.-M. Peng, X. Duan, Q. Chen, X. Liang, Microwave absorption enhancement and complex permittivity and permeability of Fe encapsulated within carbon nanotubes, Adv. Mater. 16 (2004) 401-405. https://doi.org/10.1002/adma.200306460.

[15] H. Sun, R. Che, X. You, Y. Jiang, Z. Yang, J. Deng, L. Qiu, H. Peng, Cross-stacking aligned carbon-nanotube films to tune microwave absorption frequencies and increase absorption intensities, Adv. Mater. 26 (2014) 8120-8125. https://doi.org/10.1002/adma.201403735.

[16] I. Ebrahimi, M. P.Gashti, Polypyrrole-MWCNT-Ag composites for electromagnetic shielding: Comparison between chemical deposition and UV-reduction approaches, J. Phys. Chem. Solids, 118 (2018) 80-87. https://doi.org/10.1016/j.jpcs.2018.03.008.

[17] C. Wen, X. Li, R. Zhang, C. Xu, W. You, Z. Liu, B. Zhao, R. Che, High-density anisotropy magnetism enhanced microwave absorption performance in Ti3C2Tx MXene@Ni microspheres, ACS Nano 16 (2021) 1150-1159. https://doi.org/10.1021/acsnano.1c08957.

[18] Q. Liu, Q. Cao, H. Bi, C. Liang, K. Yuan, W. She, Y. Yang, R. Che, CoNi@SiO2@TiO2 and CoNi@Air@TiO2 microspheres with strong wideband microwave absorption, Adv. Mater. 28 (2016) 486-490. https://doi.org/10.1002/adma.201503149.

[19] B. Zhao, Y. Li, Q. Zeng, L. Wang, J. Ding, R. Zhang, R. Che, Galvanic replacement reaction involving core-shell magnetic chains and orientation-tunable microwave absorption properties, Small 16 (2020). https://doi.org/10.1002/smll.202003502.

[20] B. Zhao, X. Guo, W. Zhao, J. Deng, G. Shao, B. Fan, Z. Bai, and R. Zhang, Yolk–shell Ni@SnO2 composites with a designable interspace to improve the electromagnetic wave absorption properties, ACS Appl. Mater. Interfaces 8 (2016) 28917-28925. https://doi.org/10.1021/acsami.6b10886.

[21] B. Zhao, G. Shao, B. Fan, W. Zhao, Y. Xiea, R. Zhang, Synthesis of flower-like CuS hollow microspheres based on nanoflakes self-assembly and their microwave absorption properties, J. Mater. Chem. A 3 (2015) 10345-10352. https://doi.org/10.1039/c5ta00086f.

[22] S. Kirchmeyer, K Reuter, Scientific importance, properties and growing applications of poly(3,4-ethylenedioxythiophene), J. Mater. Chem. 15 (2005) 2077–2088. https://doi.org/10.1039/B417803N.

[23] S. M. Benhamou, A. J. Lozano-Guerrero, Y. Madaoui, A. Díaz-Morcillo, M. Hamouni ,Measurement and investigation of electromagnetic shielding properties of 3,4 ethylenedioxythiophene–maghnite–Sodium, in: IEEE International Symposium on Electromagnetic Compatibility, 2018, 27-30. https://10.1109/EMCEurope.2018.8485028.

[24] A. J. Lozano Guerrero, M. P. Robinson, A. Díaz Morcillo, J. V. Balbastre Tejedor. Benefits of using conductive plastics in shielding configurations to reduce radiated electromagnetic interference, Microw. Opt. Technol. Lett. 52 (2010) 2476-2480. https://doi.org/10.1002/mop.25499.

[25] A. J. Lozano Guerrero, M. P. Robinson, A. Díaz Morcillo, J. Monzó-Cabrera, F. J. Clemente-Fernández, J. V. Balbastre-Tejedor, Shielding properties of conductive plastic housings loaded with printed circuit boards, Electromagnetics. 32 (2012) 495-505. https://doi.org/10.1080/02726343.2012.726915.

[26] M. Belbachiret A. Bensaoula, Composition and method for catalysis using bentonites; US Patent N° 7094823 (2006)

[27] A. Megherbi, R. Meghabar, M. Belbachir, Preparation and characterization of clay (maghnite-H)/poly(3,4-ethylenedioxythiophene) composites, J. Surf. Eng. Mater. Adv. Technol. 3 (2013) 21-27. https://10.4236/jsemat.2013.31004.

[28] A. Saad, K. Jlassi, M. Omastová, M. M.Chehimi, Clay/Conductive polymer nanocomposites, in Elsevier, Clay-Polymer Nanocomposites, Amsterdam, 2017, pp. 199-237.

[29] D. Azuma, Magnetic materials, in Elsevier, Wide Bandgap power semiconductor packaging, materials, components, and reliability, Amsterdam, 2018, pp. 97-107.

[30] N. Chen, G. Mu, X. Pan, K. Gan, M. Gu, Microwave absorption properties of SrFe12O19/ZnFe2O4 composite powders, Mater. Sci. Eng. B. 139 (2007) 256–260. https://doi.org/10.1016/j.mseb.2007.02.002

[31] A.J. Lozano-Guerrero, F.J. Clemente-Fernández, J. Monzó-Cabrera, J.L. Pedreño-Molina, A. Díaz-Morcillo, Precise evaluation of coaxial to waveguide transitions by means of inverse techniques, IEEE Trans. Microw. Theory. Techn. 58 (2010) 229 – 235. https://10.1109/TMTT.2009.2036408.

[32] A. McDowell, H. Hubing, Decomposition of shielding effectiveness into absorption and reflection components, Technical report: CVEL-14-058.1, Clemson University, 2016.

[33] A. Prokopchuk, I. Zozulia, Y. Didenko, D. Tatarchuk, H. Heuer, and Y. Poplavko Dielectric permittivity model for polymer–filler composite materials by the example of Ni- and graphite-filled composites for high-frequency absorbing coatings, Coatings. 11 (2021) 172 – 192. https://doi.org/10.3390/coatings11020172.

[34] A.J. Lozano-Guerrero, S. M. Benhamou. Shielding effectiveness of conductive materials and composites; in Nova Science Publishers, Conductive materials and composites, New York, 2016, pp. 91-110.